The EMBO Journal vol.14 no.12 pp.2689–2699, 1995

Crystal structure of dimeric human ciliary neurotrophic factor determined by MAD phasing

N.Q.McDonald[1,2], N.Panayotatos[3] and W.A.Hendrickson

Department of Biochemistry and Molecular Biophysics and the Howard Hughes Medical Institute, Columbia University, New York, NY 10032, USA
[1]Present address: ICRF Unit for Structural Biology, Department of Crystallography, Birkbeck College, London WC1E 7HX, UK
[3]Present address: Regeneron Pharmaceuticals Inc., Tarrytown, NY 10591-6707, USA

[2]Corresponding author

Ciliary neurotrophic factor (CNTF) promotes the survival and differentiation of developing motor neurons and is a potential therapeutic for treating neurodegeneration and nerve injury. The crystal structure of human CNTF has been determined at 2.4 Å resolution using multi-wavelength anomalous diffraction (MAD) phasing from a single Yb^{3+} ion. The structure reveals that CNTF is dimeric, with a novel anti-parallel arrangement of the subunits, not previously observed for other cytokines. Each subunit adopts a double crossover four-helix bundle fold, in which two helices contribute to the dimer interface, whilst two different helices show pronounced kinks. Analysis of the electrostatic surface of CNTF identified residues within these kinked helices that may contact the CNTF receptor-α. Solution experiments show that CNTF dimerizes at concentrations >40 μM. Such dimers are likely to be relevant to the storage of CNTF in the peripheral nerve given the high concentrations present in this tissue. However, it is unlikely that they play a role in engaging the three distinct receptor subunits that comprise the CNTF receptor, given the low concentration of extracellular CNTF and its high potency.

Key words: cytokine/multi-wavelength anomalous diffraction/neurotrophic factor/X-ray structure

Introduction

Ciliary neurotrophic factor (CNTF) supports the survival of a variety of neuronal cell types such as sensory, sympathetic, ciliary and motor neurons and also certain non-neuronal cells, including oligodendrocytes and skeletal muscle cells (Sendtner *et al.*, 1994). It is abundantly expressed within myelin-related Schwann cells associated with the peripheral nerve (Friedman *et al.*, 1992), but lacks a classical signal peptide sequence (Stockli *et al.*, 1989). Thus a role for CNTF as a neuroprotectant has been suggested whereby it is released from damaged cells to restore neuronal function after injury (Adler, 1993). CNTF is able to prevent the degeneration of motor neurons after axotomy (Sendtner *et al.*, 1990) and has been of interest therapeutically, either alone or in combination with other neurotrophic factors, for the treatment of neurodegenerative diseases (Lindsay *et al.*, 1994; Nishi, 1994). More potent forms of CNTF could thus potentially be of use clinically.

CNTF is structurally and functionally related to members of a family of cytokines that includes leukaemia inhibitory factor (LIF), interleukin-6 (IL-6), interleukin-11 (IL-11) and oncostatin M (OSM) (Sprang and Bazan, 1993; Briscoe *et al.*, 1994). These molecules have been predicted to belong to the long chain helical cytokine superfamily (Sprang and Bazan, 1993). The structure of murine LIF has recently been determined by X-ray crystallography confirming these predictions but also revealing distinctive features (Robinson *et al.*, 1994). Within the helical cytokine fold considerable diversification in the length and packing of secondary structural elements is evident from a comparison of known crystal and NMR structures (Rozwarski *et al.*, 1994). Also several cytokines are found associated as dimers either through covalent [such as macrophage colony-stimulating factor (M-CSF) and stem cell factor (SCF)] or non-covalent interactions [interferon (IFN)-β, IFN-γ and IL-5] with quite different protomer arrangements (Sprang and Bazan, 1993).

Signal transduction by CNTF requires that it bind first to a specific cell surface receptor, CNTF-Rα, permitting the subsequent recruitment of the receptors gp130 and LIF-Rβ (Stahl and Yancopoulos, 1993). It is this tripartite CNTF receptor complex that is able to activate intracellular signalling cascades (Davis *et al.*, 1993b). CNTF-Rα is linked through a glycosylphosphatidylinositol (GPI) anchor to the extracellular membrane and serves to modulate the binding properties of CNTF towards gp130 and LIF-Rβ (Davis *et al.*, 1991, 1993a). Both gp130 and LIF-Rβ are single pass transmembrane receptors that couple to Jak/Tyk kinases to activate STAT and also the ras/raf signalling cascade (Briscoe *et al.*, 1994). They are also receptors for LIF, IL-11 and OSM, whilst gp130 is one of two distinct receptor subunits for IL-6. A general characteristic of these cytokine–receptor complexes is the engagement of a cytokine-specific receptor subunit by the ligand, together with gp130 and, in some instances, additional receptor components (Stahl and Yancopoulos, 1993).

We report here the X-ray structure of a truncated form of human CNTF (residues 2–187, lacking the C-terminal 13 amino acids) phased from multi-wavelength anomalous diffraction data (MAD). The CNTF structure is compared and contrasted with other known cytokine structures, highlighting several important novel features of CNTF that may have functional consequences. We propose a model for the engagement of the various receptor subunits that comprise the CNTF receptor based on available structural and mutagenesis data for CNTF and related neurokines.

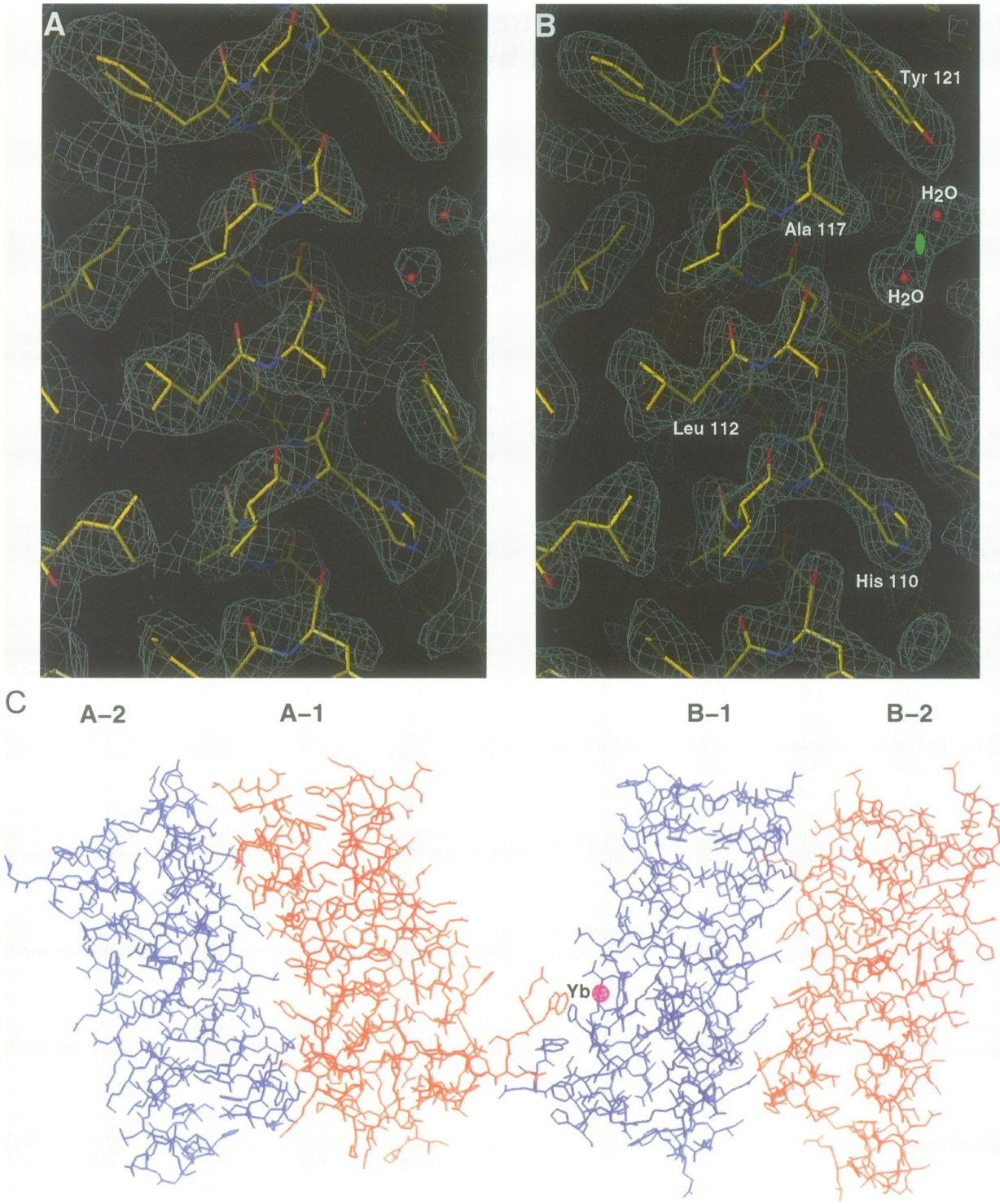

Fig. 1. (**A**) A portion of a MAD-phased experimental map calculated at 2.7 Å resolution. (**B**) The current $2|F_o|-|F_c|$ map superimposed with the model refined at 2.4 Å resolution. Electron density (contoured at 1.0σ, coloured grey) is shown for part of the C helix. The approximate position of the molecular dyad is indicated by a green ellipse located between two buried water molecules. The figure was drawn using O (Jones *et al.*, 1991). (**C**) The two non-crystallographic dimers of CNTF within the asymmetric unit. The dyad axes are approximately perpendicular to the plane of the page. The $2|F_o|-|F_c|$ electron density is shown close to the Yb^{3+} ion (purple) contoured at 8σ. Drawn using SETOR (Evans, 1993).

Results

Crystals of CNTF diffracted weakly and had a relatively large unit cell because of multiple copies of CNTF in the asymmetric unit (see Materials and methods and Figure 1C). An ytterbium-derivatized crystal of CNTF produced a single Yb^{3+} site bound at an interface between two dimers (Figure 1C). This provided a suitable means to obtain experimental phasing information by taking advantage of the large anomalous features close to the Yb L_{III} edge and applying a MAD analysis (Hendrickson, 1991). Cryo-cooling a single crystal to –150°C in paratone-N was essential to measure multi-wavelength data (Table I). A good quality electron density map was

Table I. Data collection statistics

Wavelength (Å)	Unique reflections (completeness)[a]	R_{sym} (%)[b]	Observed ratios (20.0–2.7 Å)[c]					
			λ_1	λ_2	λ_3	λ_4	f′ (e)	f″ (e)
1.3862 (inflection λ_1)	18 742 (95.5)	5.0 (13.7)	0.058 (0.032)	0.043	0.048	0.044	−28.9	11.9
1.3855 (peak λ_2)	18 780 (95.7)	5.4 (15.8)		0.096 (0.033)	0.040	0.039	−16.8	24.8
1.3848 (inflection λ_3)	18 770 (95.6)	5.1 (14.3)			0.064 (0.033)	0.035	−7.6	14.2
1.3700 (remote λ_4)	18 791 (95.7)	4.9 (13.9)				0.058 (0.032)	−10.6	10.6
1.3700 (remote λ_4) high resolution[d]	26 042 (94.5)	5.5 (28.4)						

[a]Unique reflections are determined by point group 222 (not mmm) to distinguish Bijvoet-related reflections. Each dataset had an average redundancy of 4.2.
[b]$R_{sym} = 100 \times \Sigma\Sigma|I_i - \langle I \rangle| / \Sigma\Sigma I_i$ where, I_i is the i^{th} observation and $\langle I \rangle$ is the weighted mean of all observations. Values shown are for reflections between 20 and 2.7 Å and 2.8 and 2.7 Å (in parentheses), excepting the high resolution dataset (20 to 2.4 Å and 2.5 to 2.4 Å in parentheses).
[c]Observed diffraction ratios are the Bijvoet difference ratios (diagonal elements) at each wavelength and the dispersive difference ratios (off-diagonal elements) between pairs of wavelengths. Each is calculated from $\langle \Delta|F|^2 \rangle^{1/2} / \langle |F|^2 \rangle^{1/2}$ where $\Delta|F|$ is the absolute value of either the Bijvoet or dispersive difference. Values in parentheses are for centric reflections, a measure of the noise in the anomalous signal. The scattering factors f′ and f″ shown are the final refined values.
[d]Dataset reprocessed for Bragg spacings between 20.0 and 2.4 Å for use in refinement, statistics are calculated from merging 101 761 observations.

Table II. MAD phasing and refinement statistics

MAD phasing (20.0–2.7 Å)			
$R(\|^{\circ}F_A\|) = 0.44$	$R(\|^{\circ}F_T\|) = 0.05$	$\langle \Delta(\Delta\phi) \rangle = 46.8^{\circ}$	$R(^{\circ}F_A$ model) = 0.50
Current model (6.0–2.4 Å)			
R value = 19.6%	free R value = 25.1%	r.m.s. bond lengths = 0.013 Å	r.m.s. bond angles = 1.65°

produced with the MAD phases (Figure 1A), demonstrating the applicability of MAD for determining structures of large proteins (>500 residues). This map was improved in certain regions by non-crystallographic symmetry averaging, allowing the fitting of the polypeptide chain for each protomer. Subsequently the structure was refined to an R value of 19.6% for data between 6 and 2.4 Å Bragg spacings and a free R value of 25.1% (Table II).

The dimeric structure of CNTF

The four copies of CNTF within the asymmetric unit are arranged into two dimeric anti-parallel pairs (which will be referred to as A-1, to indicate molecule 1 of dimer A, A-2, B-1 and B-2) (Figure 1C). The dimer has dimensions of ~45×45×15 Å (whilst the protomer is roughly 45×20×15 Å). Each protomer is related to its dimer mate by an almost exact dyad symmetry axis (a rotation of 178.4° and 179.7°, with a corresponding translation along the symmetry axis of 0.3 and 0.1 Å respectively for each CNTF dimer) perpendicular to the long helix bundle axis.

Dynamic light scattering experiments demonstrate that such dimers form in solution at concentrations above 0.9 mg/ml (40 μM) (data not shown), indicating a weak association constant. Despite this apparently weak affinity, the CNTF dimer interface encompasses an area that runs almost the length of the molecule burying ~1038 Å^2 from each protomer. The size of this interface is similar in magnitude to those found for other oligomers (Janin *et al.*, 1988; Jones and Thornton, 1995).

Contacts within each dimer are made primarily by residues within the C helix and by several residues located on the B helix (Figure 3). Contributions to the interface are made by hydrophobic, polar and charged residues (Figure 2C). The latter tend to cluster within a narrow strip that traverses across the interface, whilst the hydrophobic and polar contacts are positioned within a prominent 'face' along the C helix axis (Figure 2C). Thus helix C has only 17% of its surface area solvent accessible in the dimer. Two water molecules are buried at the interface which form hydrogen bonds to the side chain of His84 and Tyr121 (Figure 1C). Nearly all interface side chains are conserved amongst CNTF sequences from different species (except Gln95). However, these sequences are not conserved amongst other related neuropoietic cytokines such as LIF, IL-6 and OSM.

Structural relationship of CNTF with other helical cytokines

The CNTF protomer adopts the four-helix bundle cytokine topology (Bazan, 1991), consisting of four helices (A–D) that are arranged in a left-handed, anti-parallel manner connected by two long crossover links and one short loop. Comparison of CNTF with structures of LIF, growth hormone (GH) and granulocyte (G)-CSF show that each helix is of a comparable length to its equivalent (except the shorter D helix of LIF, see below) and with similar packing arrangements and similar interhelical angles (Figure 4A and B). The most closely conserved interhelical angles between these structures are those of the C helix (mean values of 20.2 ± 1.5° and 29.7 ± 1.3° respectively for the BC and CD angles). The A helix shows the greatest variation (mean values of 37.9 ± 7.8° and 34.7 ± 11.0° respectively for the AB and AC angles) and is particularly evident in the CNTF–LIF comparison (Figure 4B). The best overall superposition of CNTF is with G-CSF (85 Cα atoms superposed with an r.m.s. deviation of 1.05 Å).

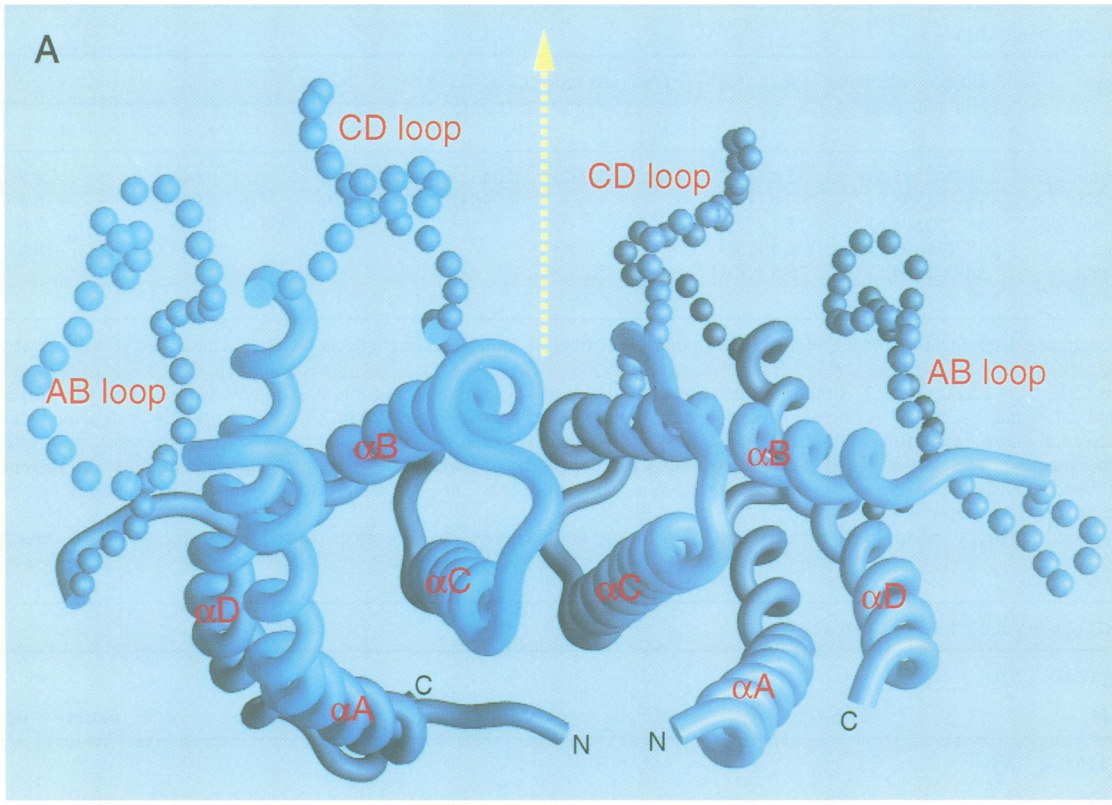
A
CD loop
CD loop
AB loop
AB loop
αB
αB
αC
αC
αD
αD
αA
αA
C
N
N
C

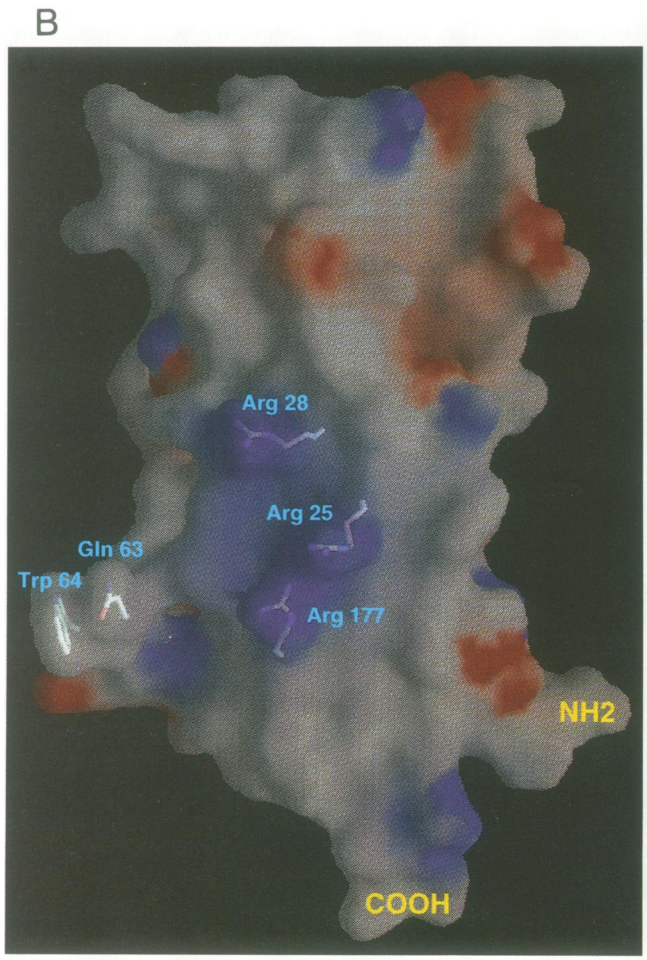
B
Arg 28
Arg 25
Gln 63
Trp 64
Arg 177
NH2
COOH

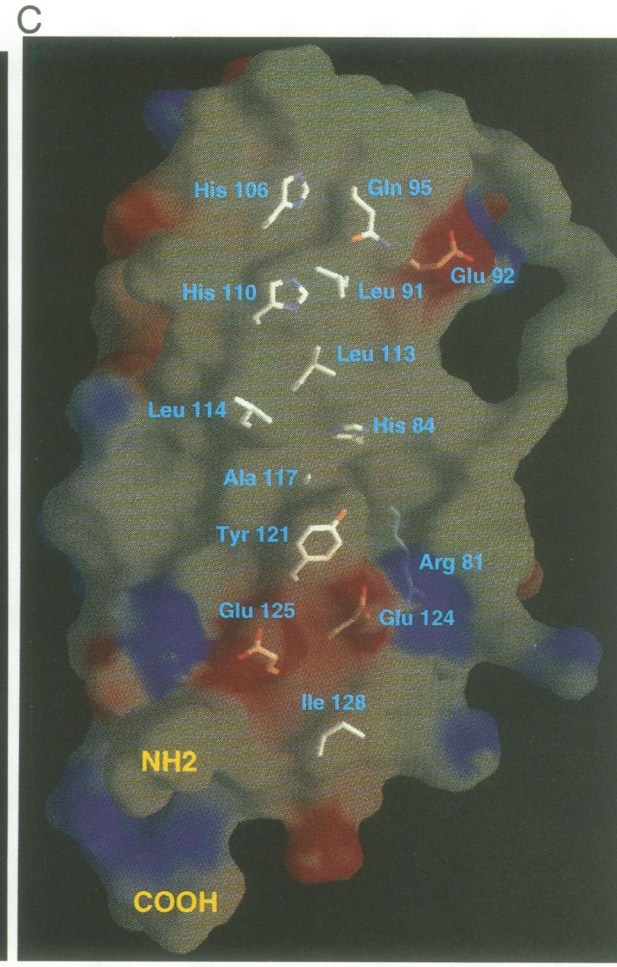
C
His 106
Gln 95
Glu 92
His 110
Leu 91
Leu 113
Leu 114
His 84
Ala 117
Tyr 121
Arg 81
Glu 125
Glu 124
Ile 128
NH2
COOH

The variation in angles for the A helix and also the D helix is due to a feature that may be specific to the neuropoietic cytokines. Both helices point away from the dimer interface and have their regular main chain hydrogen bonding patterns disrupted by a kink in the middle of each (Figure 2A). In both cases, the Oγ1 atom of a threonine side chain (Thr32 for helix A and Thr169 for helix D), together with several water molecules, hydrogen bond to the unsatisfied main chain amide and carbonyl functions created by the kink. A kink is found at a similar, though not identical, position in the A and D helices of LIF (Robinson *et al.*, 1994). However, LIF utilizes the Oγ atom of a serine residue (Ser36 for the helix A, corresponding to Asp30 of CNTF, and Ser164 for helix D) and a number of water molecules to satisfy the unfulfilled main chain hydrogen bonding donors and acceptors (Robinson *et al.*, 1994).

Both CNTF and LIF have shorter AB loops than GH or G-CSF. A large part of this loop and approximately half of the CD loop are poorly ordered for each copy of CNTF, a feature that has been observed previously in the structures of both GH and G-CSF (Hill *et al.*, 1993; Ultsch *et al.*, 1994). In contrast, the conformation of the AB loop of LIF is well defined by the LIF crystal structure, possibly because of a disulphide bridge that tethers the AB loop to the D helix (Robinson *et al.*, 1994). A short mini-helix observed within the AB loop of LIF is likely to be preserved in CNTF, based on the conservation of the primary sequence in this region (residues 50–53, Figure 3); however, no convincing electron density is evident for this segment. The C-terminal end of the AB loop is extended away from the helical bundle core compared with the murine LIF AB loop with Trp64 of CNTF A-1 protomer lying 12.1 Å distal to the structurally equivalent residue Phe70 of LIF (Figure 4B).

Two further unique features of CNTF are the long BC loop and a sequence extension of 20 residues beyond helix D at the C-terminus. At least 13 of these residues can be removed from CNTF without loss of activity (see Materials and methods). The D helix of CNTF is comparable in length with that of G-CSF and GH and is approximately two turns of helix longer than that of LIF (Robinson *et al.*, 1994).

Conformational flexibility of CNTF

The poor density observed for the AB and CD loops of CNTF and the high average atomic B factor of 36 Å^2 (despite cryo-cooling conditions) suggests a highly flexible molecule. Indeed the B-1 protomer has an average B factor of 42 Å^2, explaining the poorer density generally found for this molecule. Superposing the four CNTF protomers highlights the rigidity of the four-helix bundle core and the relative plasticity of other regions (Table III). A large structural difference is found for residues 63–68 of the A-1 and B-1 protomers (Figure 2D), with a main chain shift of 4.6 Å between the Trp64 Cα atom of each molecule. This shift arises from a rotation about several main chain torsion angles up to the φ torsion angle for residue 66 and can be attributed to lattice contacts. No density is observed for equivalent regions in A-2 and B-2, which make no lattice contacts. These conformational differences of A-1 and B-1 are of interest in the light of mutagenesis data indicating that Gln63 and Trp64 define part of the CNTF-Rα site (Panayotatos *et al.*, 1993, 1995). For B-1, the Trp64 indole ring nitrogen (Nε1) hydrogen bonds to Oδ1 of Asp175 whereas for A-1, the Trp64 indole ring stacks against the aromatic ring of His174 from a symmetry-related molecule (Figures 1C and 2D). It is not clear whether this conformational change represents two specific conformers used to switch between a free and receptor-bound ligand conformation or two arbitrarily stabilized conformers out of a range of possible structures.

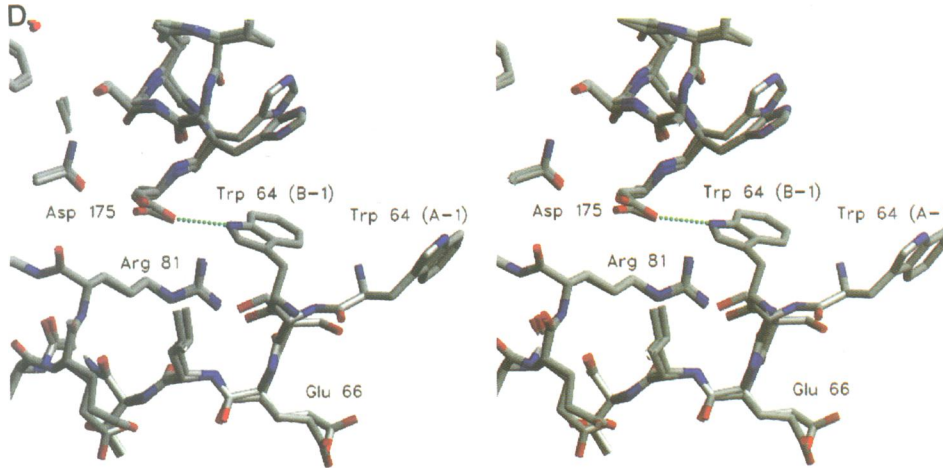

Fig. 2. (**A**) A schematic fold of the CNTF dimer (molecule A-1 in blue and A-2 in light blue). The secondary structural elements are labelled for each protomer. The dyad axis is represented by a dashed arrow. Spheres are shown to represent the poorly ordered portions of the AB and CD loops (residues 45–62 and 140–151). Alternate spheres along the chain represent Cα positions. The N-terminal 11 residues are disordered in A-1 and A-2, in addition to residues 181–187 from A-2. (**B**) and (**C**) Electrostatic surface of the CNTF protomer (blue represents positive potential and red negative), calculated without the ytterbium ion, the sulphate or water molecules. The Cα trace of the poorly ordered parts of the the AB loop and CD loop were included in the surface calculation. (B) highlights a positive cluster of three arginine residues (Arg25, Arg28 and Arg177) shown only as side chains close to Gln63 and Trp64, each of which has been implicated in binding CNTF-Rα (Panayotatos *et al.*, 1993, 1995). (C) Residues buried within the CNTF dimer interface. (**D**) Conformational differences between molecules A-1 and B-1 in the region close to Trp64. A, B and C were made using GRASP (Nicholls *et al.*, 1991), D was made using SETOR (Evans, 1993).

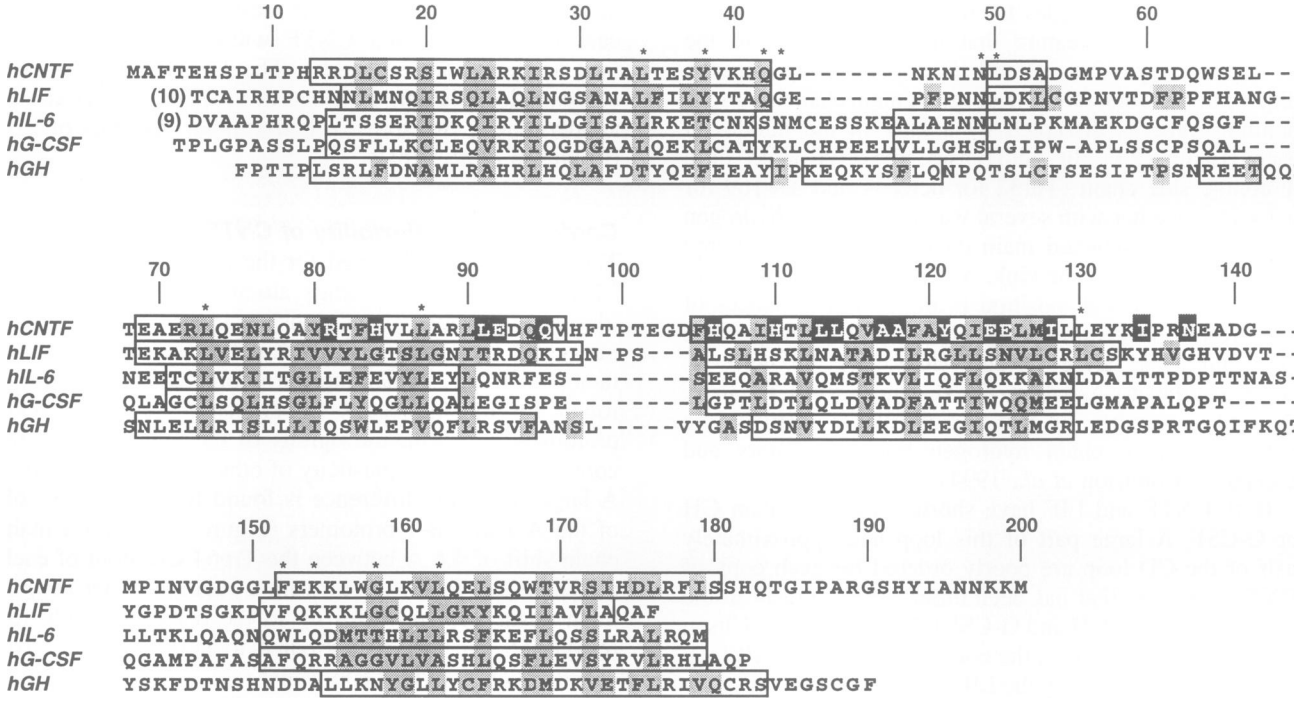

Fig. 3. Structure-based alignment of CNTF with representative members of the neuropoietic cytokines (LIF and IL-6) and the long chain helical cytokine families (GH and G-CSF). Murine LIF, human GH and murine G-CSF structures were aligned with CNTF through structural superposition using the TOSS procedure (Hendrickson, 1979) by including a framework of Cα positions associated with the four-helix bundle. Coordinates sets of G-CSF (entry name 1RHG) and GH (entry name 3HHR) from the Protein Data Bank were used. Murine LIF coordinates were obtained from Drs R.Robinson and Y.Jones (Oxford University). Cα atoms were included if within 2 Å of their counterparts after the superposition. Sequences shown are for the human variants of each cytokine; the human IL-6 sequence was aligned by hand. 85 Cα atoms of CNTF and G-CSF superposed with an r.m.s. deviation of 1.05 Å, whilst 67 Cα atoms of CNTF and GH gave an r.m.s. deviation of 1.16 Å. 70 Cα atoms of CNTF and LIF superpose with an r.m.s. of 1.09 Å. Grey indicates solvent-inaccessible residues; reverse contrast indicates residues at the dimer interface. Asterisks indicate conserved residues in the majority of neuropoietic cytokine sequences. Helical secondary structure assignments are shown as boxes enclosing the appropriate residues. Residues 50–53 of CNTF are predicted to form a mini-helix based on the structure of LIF and from the sequence conservation between these two molecules, despite the absence of interpretable density for this region. Predicted helices of IL-6 were based on the alignment and similarity to G-CSF.

Evolutionary relationships amongst neuropoietic cytokines

Only 12 residues in CNTF are highly conserved amongst those cytokine sequences sharing a gp130-binding function (Figure 3), the majority of which cluster close to one part of the CNTF core. Leu34, Leu87 and Leu162 all make intimate contact within the helix bundle core. Two pairs of residues appear to be conserved in a correlated fashion, based on alignments of neurokine sequences. An explanation for their conservation is evident from the CNTF structure; Lys155 side chain hydrogen bonds to Oε1 of Gln42, whilst Gly158 packs against the Tyr38 side chain, with no room available for a Cβ atom. Replacing Gly158 by Ala renders CNTF inactive (Panayotatos *et al.*, 1995), most likely due to perturbation of the CNTF structure. Two other residues, Gly43 and Glu131, are not conserved amongst other neuropoietic cytokines but their positive φ torsion angles are. These residues are found at the C-terminal end of the A and C helices respectively, and most probably serve to terminate each α-helix. Structural counterparts are found for G-CSF (Lys40 and Gly125) and for LIF (Gly49–Cys134 is found in place of Glu131 of CNTF).

The preservation of the core residues supports a proposed homologous relationship between these molecules that was based on their similar intron/exon boundaries and low but significant level of sequence similarity (Bazan, 1991). Amongst the wider superfamily of helical cytokines, essentially no sequence identity can be found, despite the common structural framework (Figure 3) and the closer fit observed between CNTF and G-CSF, rather than LIF (Figure 3 legend).

Identification of a functionally important cluster of arginine residues

Analysis of the electrostatic surface of CNTF indicates a cluster of three Arg residues (Arg25, Arg28 and Arg177) that are highly conserved amongst CNTF sequences. Each is accessible to solvent and lies close to Gln63, previously identified as a key CNTF-Rα binding determinant (Figure 2B). Such patches of electrostatic potential have been implicated in determining cytokine and neurotrophic factor receptor specificity (Ibanez *et al.*, 1992; Demchuk *et al.*, 1994). These residues were substituted for alanine (as described elsewhere; Panayotatos *et al.*, 1995) and had a reduced affinity for CNTF-Rα and a lower bioactivity on embryonic ciliary neurons. Thus, this prominent cluster of three Arg residues would seem to play an important role in binding CNTF-Rα together with residues Gln63 and Trp64 of the AB loop (Panayotatos *et al.*, 1995). We note that the positioning of these residues in the A and D

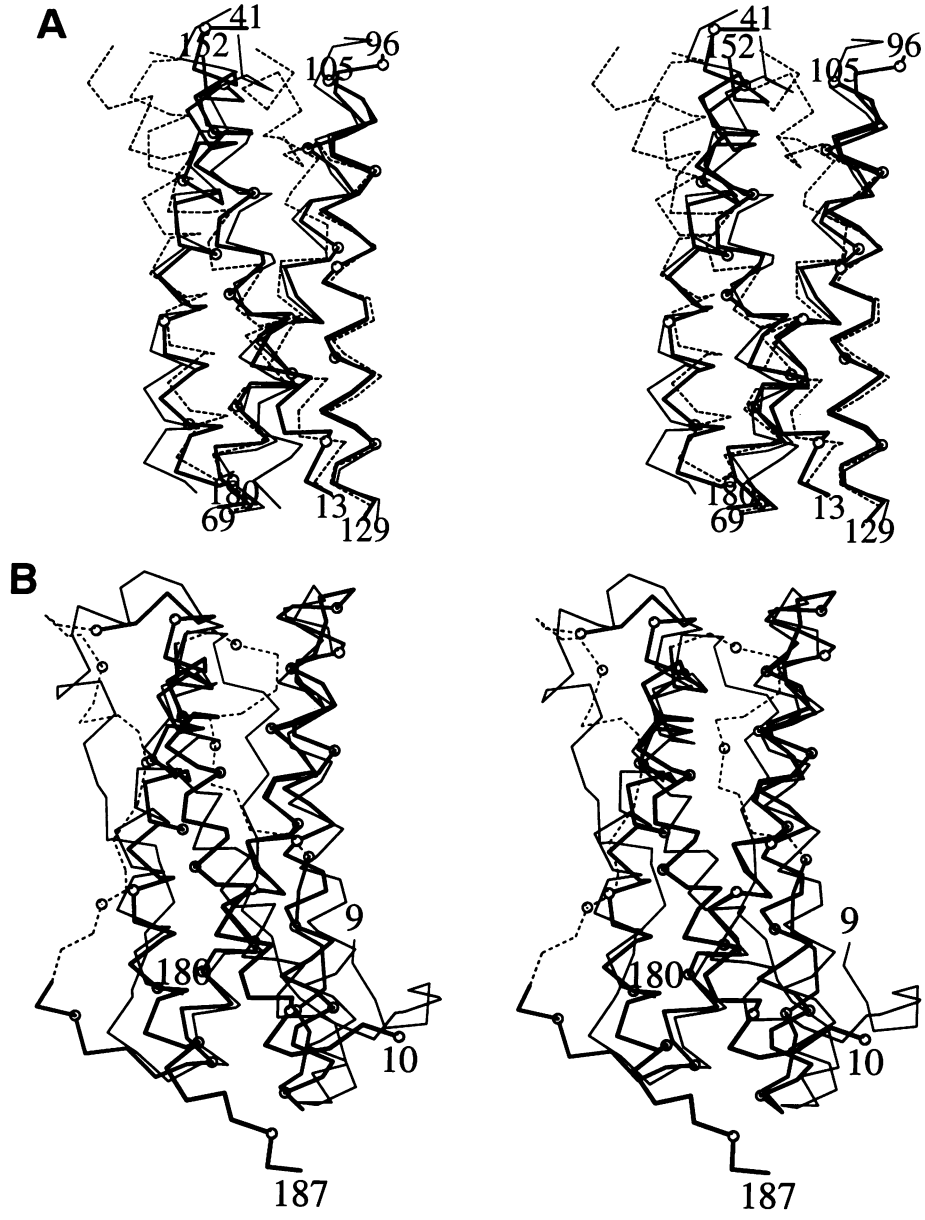

Fig. 4. (**A**) A stereo Cα trace of the four-helix bundle core of CNTF protomer A-1 (bold), superposed with the long helical cytokines G-CSF (thin) and GH (dashed) according to the alignment of Figure 3. The N- and C-terminal residues of each helix of CNTF are labelled. White balls are shown for the Cα position of every fifth residue in CNTF. (**B**) A stereo Cα trace of CNTF A-1 (bold) superposed with the neuropoietic cytokine LIF (thin). The N- and C-termini are labelled for CNTF (residues 10 and 187) and for LIF (residues 9 and 180). The poorly ordered portions of the AB and CD loop of CNTF are shown as dashed lines. This figure was produced by MOLSCRIPT (Kraulis, 1991).

helices and the AB loop is analogous to those from the high affinity site of GH (De Vos *et al.*, 1992).

Discussion

Despite the large asymmetric unit and fragile nature of the crystals of CNTF, a MAD phasing approach was successful in producing a high quality electron density map from data obtained from a single crystal. The large Bijvoet and dispersive differences observed for the single site CNTF derivative suggest lanthanide elements are well suited to tackling large macromolecular structures if suitable sites can be identified either empirically, as shown here, or through the substitution of intrinsic calcium or magnesium ions (Weis *et al.*, 1991; Shapiro *et al.*, 1995).

Table III. R.m.s. differences (Å) between the various CNTF protomers, for the four-helix bundle core (98 Cα positions) (upper right corner) and for all Cα atoms (lower left corner)

	A-1	A-2	B-1	B-2
A-1	x	0.45	0.26	0.34
A-2	0.70 (122 Cα)	x	0.42	0.51
B-1	0.63 (140 Cα)	0.70 (128 Cα)	x	0.36
B-2	0.46 (126 Cα)	0.82 (123 Cα)	0.47 (125 Cα)	x

The unexpected arrangement of the four CNTF molecules into two dimers has shown for the first time the ability of CNTF to oligomerize in a highly specific manner that may have a biological role. Importantly, the

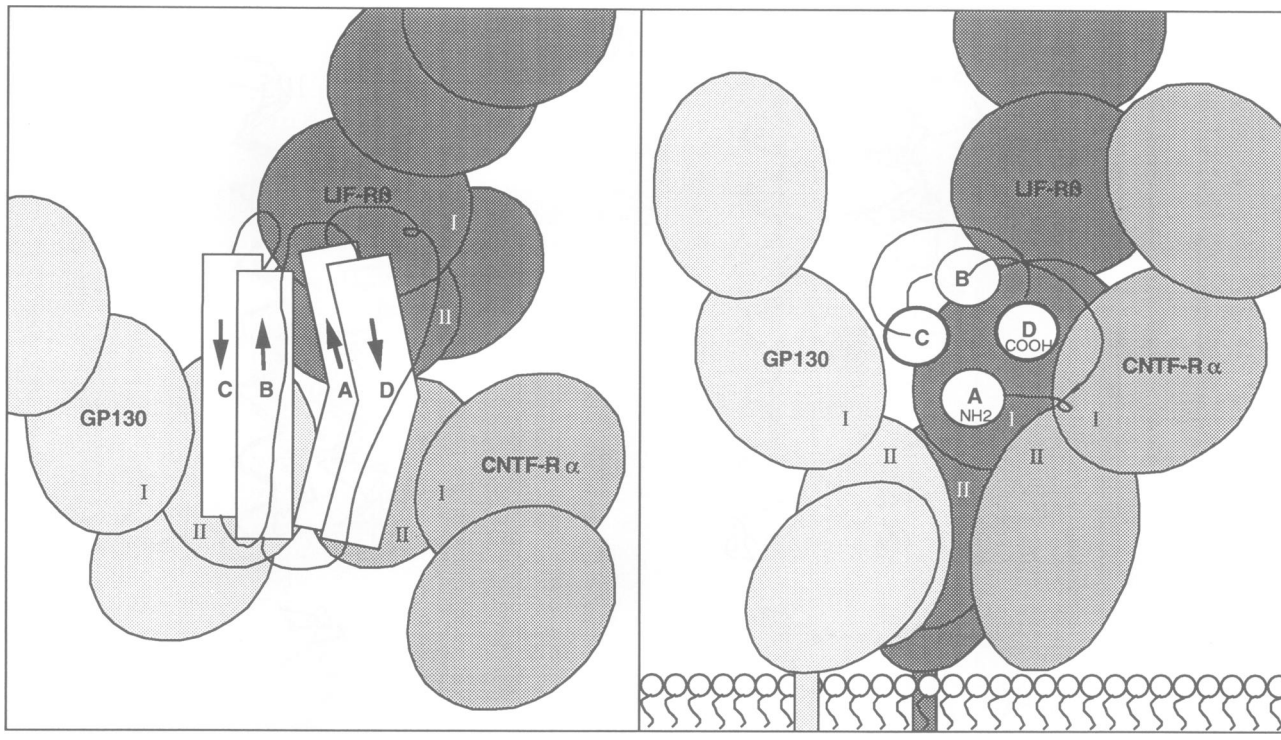

Fig. 5. Two orthogonal views of a highly schematized model of the tripartite CNTF receptor viewed either above the cell membrane (left hand side) or perpendicular to it (right hand side). The shaded ellipsoids represent the multiple extracellular domains (typically fibronectin type III-like) of each receptor component. gp130 and LIF-Rβ are predicted to have four and six identifiable domains respectively, whilst CNTF-Rα is likely to have three such domains (Kossiakoff *et al.*, 1994; Mott and Campbell, 1995). This model makes the following assumptions: the CNTF monomer is the biologically active moiety based on the low extracellular concentration of CNTF (Sendtner *et al.*, 1992) and the 1:1 stoichiometry of the CNTF/CNTF-Rα complex observed in solution (Panayotatos *et al.*, 1994); the region of each receptor subunit homologous to the growth hormone receptor is assumed by analogy to be important for interaction with the CNTF ligand. This comprises a fibronectin type III domain with a conserved disulphide pattern shared by class 1 cytokine receptors (indicated by I) and a 'WSXWS' fibronectin type III module (indicated by II), collectively known as the cytokine receptor module (Kossiakoff *et al.*, 1994). Both gp130 and LIF-Rβ are likely to have an additional fibronectin type III domain between the cytokine receptor module and the transmembrane portion. Based on these assumptions and available mutagenesis data for CNTF (Panayotatos *et al.*, 1993, 1995), IL-6 (Leebeeck *et al.*, 1992; Fontaine *et al.*, 1993; Savino *et al.*, 1993, 1994; Ehlers *et al.*, 1994) and LIF (Owczarek *et al.*, 1993; Robinson *et al.*, 1994), we have positioned the CNTF-Rα at a site equivalent to site 1 of growth hormone (De Vos *et al.*, 1992), gp130 at site 2 of growth hormone and LIF-Rβ positioned close to the BC and CD loops.

participation of the B and C helices at the dimer interface is a unique mode of dimerization distinct from other helical cytokines known to act physiologically as dimers, and which use either different helices or intermolecular disulphide bridges between connecting loops (Ealick *et al.*, 1991; Pandit *et al.*, 1992; Milburn *et al.*, 1993) to stabilize their respective dimers.

The low, almost undetectable, amounts of extracellular CNTF found *in vivo* and the high potency of CNTF both suggest that the active form of CNTF is monomeric. The high protein concentrations used for crystallization could have produced an artificial association, as has been found in other cases (Baldwin *et al.*, 1991; Rajarathnam *et al.*, 1994). However, given the higher concentrations of CNTF in the peripheral nerve (Williams *et al.*, 1984), the CNTF dimer may serve as a storage form analogous to the dimeric form of growth hormone which is found in storage granules prior to release to the pituitary gland (Cunningham *et al.*, 1991). Such CNTF dimers may provide additional stability to the intracellular stores of CNTF within Schwann cells and would be able to dissociate into active monomers following nerve injury and release of CNTF into an extracelllar environment.

Another plausible role for the CNTF dimer could be to cluster receptor subunits that comprise the multicomponent CNTF receptor. Though the stoichiometry of the various receptor subunits and CNTF within the high affinity CNTF receptor is not known, CNTF has been shown to bind CNTF-Rα with a 1:1 stoichiometry in solution (Panayotatos *et al.*, 1994). We therefore believe it is unlikely that these dimers are involved in receptor activation, though further experiments are necessary to demonstrate this. On the other hand, precedents do exist for multimeric forms of helical cytokines participating in receptor activation (IL-5, IL-3, M-CSF) and we note that IL-6 has also been reported to form oligomers (May *et al.*, 1991). Moreover, investigation of the high affinity IL-6 receptor reveals a hexameric complex comprised of two IL-6, two IL-6-Rα and two gp130 molecules (Ward *et al.*, 1994).

The lack of conservation of dimer interface residues for CNTF with other neurokines suggests that dimerization is specific to CNTF, and indeed, dimeric forms of LIF have not been observed in solution or within crystals (Robinson *et al.*, 1994). Although the neuropoietic cytokines share similar topological folds to those of other helical cytokines, subtle differences such as the kinked A and D helices found in CNTF and LIF are likely to be specific to the neurokines. These three-dimensional features may well play a functional role in delineating distinct sites for the various shared receptor components of the neurokine family. Generally, it is these A and D

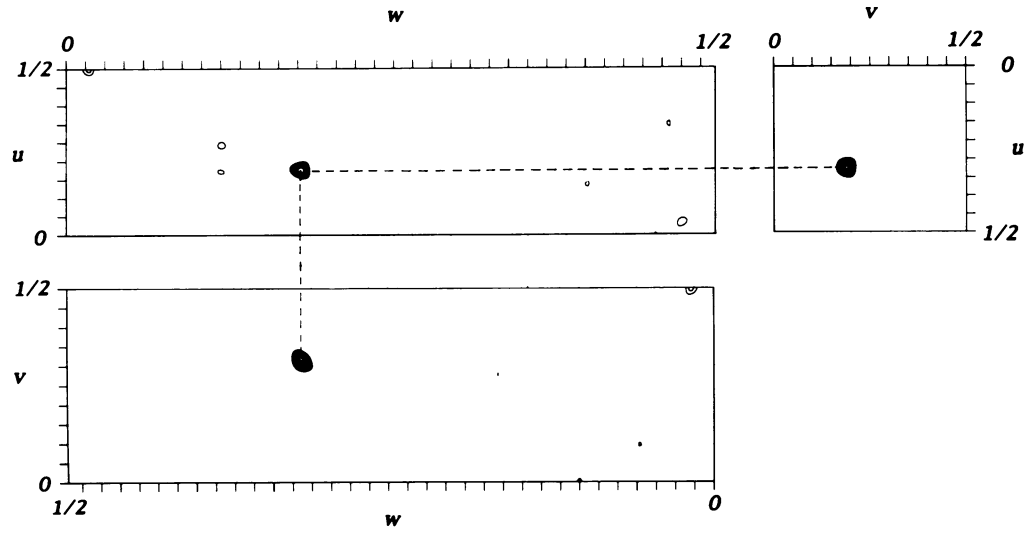

Fig. 6. Harker sections from a Bijvoet difference Patterson map for the ytterbium trichloride derivative, calculated using data from the 1.3855 Å peak wavelength. The dashed line indicates the relationship between the three self-Harker vectors in defining a single Yb^{3+} site. The map is contoured in intervals of one σ, starting at two σ.

helices that show the greatest variation in their orientation and length, as judged by least squares superpositioning of cytokine structures.

The involvement of positively charged side chains within the A and D helices in the interaction between CNTF and CNTF-Rα is reminiscent of the p75 receptor epitope of nerve growth factor and related neurotrophins (Ibanez *et al.*, 1992; Ryden *et al.*, 1995). Use of long range electrostatic forces are likely to be important for recruiting the limited amounts of such ligands and localizing them at the cell membrane, facilitating the binding of the signal transducing receptor subunits, such as gp130 and LIF-Rβ.

Current mutagenesis data are consistent with a structural equivalence of receptor binding epitopes between the neurokines and haematopoietic cytokines such as GH (De Vos *et al.*, 1992; Savino *et al.*, 1993, 1994; Robinson *et al.*, 1994; Panayotatos *et al.*, 1995). Generally, the cytokine-specific receptor epitope comprises a surface on the cytokine that includes part of the A and D helices and also the AB loop, whilst a second lower affinity epitope is positioned on a different face of the A helix and part of the C helix (Figure 5). Further complexity is apparent for certain neurokines due to the presence of additional receptor subunits (three for CNTF), multiple contacts by individual receptor subunits (such as proposed for LIF, Robinson *et al.*, 1994) and, in some instances, two identical receptor subunits making quite different contacts with the cytokine (such as IL-6; Ehlers *et al.*, 1994). Exceptions to the GH paradigm for receptor engagement by helical cytokines are known, for example, the IL-2 epitope for the IL-Rα subunit (Zurwaski *et al.*, 1994) and the use of covalent or non-covalent dimers of various cytokines to aggregate receptor subunits (Sprang and Bazan, 1993).

In Figure 5 we speculate as to the positioning of the various CNTF receptor subunits in relation to a CNTF monomer. The localization of part of the CNTF-Rα epitope to an accessible surface constituting portions of the A and D helices, just prior to the deviation introduced by their respective kinks (Figure 5), is at an equivalent position to the GH site 1. This may allow the accessible surface of the A and D helices beyond the kinks (residues 31–44 and 152–169), close to the BC and CD loops, to participate in binding a second receptor component, such as LIF-Rβ (Figure 5). Such a region has been proposed to form part of the LIF-Rβ epitope for LIF (Owczarek *et al.*, 1993; Robinson *et al.*, 1994); furthermore, IL-6 has one of its two gp130 binding sites located close to this position (Ehlers *et al.*, 1994).

Identification of the epitope for gp130, which is a shared receptor for all of the neurokines, is hampered by the lack of conserved surface residues between the neuropoietic cytokine sequences. Perhaps the key conserved contacts are made between receptor subunits once ligand has bound. Mutagenesis data for CNTF suggests that Lys26 and Asp30 on helix A contribute to the gp130 receptor epitope (Panayotatos *et al.*, 1995), as do the equivalent residues Tyr31 and Gly35 of IL-6 (Savino *et al.*, 1994). Both pairs of residues are located at a region similar to site 2 of GH (De Vos *et al.*, 1992), thus we position gp130 accordingly in Figure 5. In the case of CNTF, the dimer interface found in our crystals would partially occlude these residues, arguing against this CNTF dimer being biologically active.

Further high resolution epitope mapping is required to establish how far the similarities in receptor engagement extend between the neurokine and haematopoietic cytokines, for either the cytokine-specific receptor component(s) or for the gp130 receptor. The availability of the structure of CNTF will help guide such experiments and will provide a rational basis for testing the biological role of the CNTF dimer. Such information may lead to the production of potent CNTF agonists and antagonists suitable for therapeutic intervention. Such molecules could potentially be targeted towards other neurokine receptor pathways by their interaction with gp130.

Materials and methods

Protein production and crystallization

Recombinant human CNTF, lacking the C-terminal 13 residues, was purified and refolded from *Escherichia coli* according to Masiakowski *et al.* (1991). This shortened form of human CNTF had an improved stability and solubility profile and showed identical biological activity

relative to the full length molecule (Panayotatos *et al.*, unpublished data). Crystals of CNTF were readily obtained (dimensions of 0.5×0.3×0.3 mm) by vapour diffusion in hanging drops containing equal volumes of 10 mg/ml of protein solution and a reservoir solution of 7.5% PEG 8000, 0.15 M ammonium sulphate, 2 mM DTT, 50 mM sodium citrate at pH 6.35. They were subsequently transferred to stabilization buffer (0.15 M ammonium sulphate, 15% PEG 8000, 50 mM Tris–acetate at pH 6.3). The crystals belong to the space group $P2_12_12_1$ with unit cell dimensions of 62.09×208.89×52.95 Å. The crystals diffract to Bragg spacings of 2.4 Å and have four molecules within the asymmetric unit.

Diffraction measurements and cryo-cooling

Data were measured at four wavelengths from a single ytterbium-derivatized crystal of CNTF cryo-cooled to −150°C in paratone-N (Exxon). The crystal had previously been soaked for 24 h in stabilizing solution that contained 10 mM $YbCl_3$. The wavelengths were chosen based on an X-ray fluorescence spectrum from the crystal, close to the ytterbium L_{III} edge. X-ray data were recorded on Fuji imaging plates at beam line X4A of the National Synchrotron Light Source, Brookhaven National Laboratory. The imaging plates were digitized using a Fuji scanner. Data were integrated using DENZO (written by Dr Z.Otwinowski, UTSW) and then reduced using the CCP4 programs ROTAVATA and a modified version of AGROVATA (CCP4, 1994).

Phase determination by MAD analysis

Determination of the Yb coordinates was made by inspecting Harker sections from a Bijvoet difference Patterson map, calculated from the 1.3855 Å peak wavelength dataset (Figure 6). Subsequently, the data were passed through the MADSYS set of programs for phase determination from multi-wavelength data (available from W.A.H.). The merging statistics from the MAD phasing are shown in Table II. $R(|^{\circ}F_A|)$, $R(|^{\circ}F_T|)$ and $\Delta(\Delta\phi)$ are calculated from 40 431 independent evaluations for 18 227 unique reflections (92.84%) from the MAD least-squares fitting. $^{\circ}F_T$ and $^{\circ}F_A$ are the structure factors due to normal scattering from all the atoms and the anomalous scatterers respectively. $R(|^{\circ}F_i|) = \Sigma\Sigma|F_i - \langle F\rangle|/\Sigma\Sigma F_i$ where F_i is the i^{th} determination and $\langle F\rangle$ is the weighted mean of all evaluations. $\Delta\phi$ is the phase difference between $^{\circ}F_T$ and $^{\circ}F_A$. $\langle\Delta(\Delta f)\rangle$ is the average difference between independent determinations of $\Delta\phi$. $R(^{\circ}F_A \text{ model}) = \Sigma||^{\circ}F_A| - |^{\circ}F_{A,calc}|| / \Sigma|^{\circ}F_A|$ where $|^{\circ}F_{A,calc}|$ is the structure factor calculated from the anomalous scattering model. The experimental electron density map was calculated using MAD-derived phases for reflections from 20 to 2.7 Å. This map was improved in parts by averaging the electron density for the four unique CNTF molecules using LSQRHO (W.A.H.). Both electron density maps were used to trace the polypeptide chain for each molecule using a Silicon Graphics Iris workstation running the program FRODO (Jones, 1985).

Structure refinement

For refinement purposes, the remote wavelength was reprocessed to 2.4 Å. Least squares and simulated annealing refinement were carried out using X-PLOR (Brünger, 1992) against data between 6.0 and 2.4 Å. A correction for the anomalous scattering of the ytterbium ion was applied to its scattering factor. Non-crystallographic symmetry restraints were applied only during the initial rounds of refinement. The thermal restraints used gave r.m.s. deviations of 2.0 $Å^2$ for main chain-bonded atoms and 3.35 $Å^2$ for side chains. The current model has 4813 non-hydrogen atoms and includes 546 residues, one Yb^{3+} ion, two sulphate molecules and 203 water molecules.

The Yb^{3+} ion is apparently coordinated by a water molecule and five oxygen atoms, two of which are from a sulphate molecule that binds to Arg25, Arg28 and Arg177 of molecule B-1 and the remainder are donated by the side chains of Glu160 and Gln167 from a symmetry-related molecule of A-2. Density for a further potential ligand close to the Yb^{3+} ion is evident but has not currently been modelled. Only one non-glycine residue, Glu131, is outside of allowed regions of the Ramachandran plot. Residues missing from the current model include: the N-terminus (residues 1–11), the AB loop (residues 45–62) and the C-terminal portion of the CD loop (residues 141–151) for each molecule. Residues 63–66 and 181–187 are absent from molecules A-2 and B-2, whilst the residues 96–105 are poorly defined for A-2 and B-2. The atomic coordinates of CNTF have been deposited in the Brookhaven Protein Database.

Acknowledgements

We thank C.Ogata, A.DiGabriele, C.Bingman and O.Gurel for help in data collection; Y.Cong for help with protein purification; S.Hubbard, H.Yamaguchi and A.Nicholls for useful discussions. This work was supported in part by the NIH (GM3410), by the NSF (DMB89) and by the Lucille P.Markey Foundation. Beamline X4A at the National Synchrotron Light Source, a DOE facility, is supported by the Howard Hughes Medical Institute. N.Q.M. is a Lucille P.Markey UK Visiting Fellow.

References

Adler,R. (1993) *Curr. Opin. Neurobiol.*, **3**, 785–789.
Baldwin,E.T. *et al.* (1991) *Proc. Natl Acad. Sci. USA*, **88**, 502–506.
Bazan,J.F. (1991) *Neuron*, **7**, 197–208.
Briscoe,J., Guschin,D. and Muller,M. (1994) *Curr. Biol.*, **4**, 1033–1035.
Brünger,A.T. (1992) *X-PLOR; a System for X-ray Crystallography and NMR. Version 3.1.* Yale University Press, New Haven, CT.
Collaborative Computational Project Number 4 (1994) *Acta Crystallogr.*, **D50**, 760–763.
Cunningham,B.C., Mulkerrin,M.G. and Wells,J.A. (1991) *Science*, **253**, 545–548.
Davis,S., Aldrich,T.H., Valenzuela,D.M., Wong,V., Furth,M.E., Squinto,S.P. and Yancopoulos,G.D. (1991) *Science*, **253**, 53–63.
Davis,S. *et al.* (1993a) *Science*, **259**, 1736–1739.
Davis,S., Aldrich,T.H., Stahl,N., Pan,L., Taga,T., Kishimoto,T., Ip,N. and Yancopoulos,G.D. (1993b) *Science*, **260**, 1805–1808.
Demchuk,E., Mueller,T., Oschkinat,H., Sebald,W. and Wade,R.C. (1994) *Protein Sci.*, **3**, 920–935.
De Vos,A.M., Ultsch,M. and Kossiakoff,A.A. (1992) *Science*, **255**, 306–312.
Ealick,S.E., Cook,W.J., Vijay-Kumar,S., Carson,M., Nagabhushan,T.L., Trotta,P. and Bugg,C.E. (1991) *Science*, **252**, 698–702.
Ehlers,M., Grotzinger,J., deHon,F.D., Mullberg,J., Brakenhoff,J.P.J., Liu,J., Wollmer,A. and Rose-John,S. (1994) *J. Immunol.*, **153**, 1744–1753.
Evans,S.V. (1993) *J. Comp. Graph.*, **11**, 134–138.
Fontaine,V., Savino,R., Arcone,R., DeWitt,L., Brakenhoff,J.P.J., Content,J. and Ciliberto,G. (1993) *Eur. J. Biochem.*, **211**, 749–755.
Friedman,B. *et al.* (1992) *Neuron*, **9**, 295–305.
Hendrickson,W.A. (1979) *Acta Crystallogr.*, **A35**, 158–163.
Hendrickson,W.A. (1991) *Science*, **254**, 51–58.
Hill,C.P., Osslund,T.D. and Eisenberg,D. (1993) *Proc. Natl Acad. Sci. USA*, **90**, 5167–5171.
Ibanez,C.F., Ebendal,T., Barbany,G., Murray-Rust,J., Blundell,T.L. and Persson,H. (1992) *Cell*, **69**, 329–341.
Janin,J, Miller,S. and Chothia,C. (1988) *J. Mol. Biol.*, **204**, 155–164.
Jones,S. and Thornton,J.M. (1995) *Prog. Biophys. Mol. Biol.*, in press.
Jones,T.A. (1985) *Methods Enzymol.*, **115**, 157–165.
Jones,T.A., Zou,J.-Y., Cowan,S.W. and Kjeldgaard,M. (1991) *Acta Crystallogr.*, **A47**, 110–119.
Kossiakoff,A.A., Somers,W., Ultsch,M., Andow,K., Muller,Y.A. and De Vos,A.M. (1994) *Protein Sci.*, **3**, 1697–1705.
Kraulis,P. (1991) *J. Appl. Crystallogr.*, **24**, 946–950.
Leebeeck,F.W.G., Kariya,K., Schwabe,M. and Fowlkes,D.M. (1992) *J. Biol. Chem.*, **267**, 14832–14838.
Lindsay,R.M., Wiegand,S.J., Altar,C.A. and Distefano,P.S. (1994). *Trends Neurosci.*, **17**, 182–190.
Masiakowski,P. *et al.* (1991) *J. Neurochem.*, **57**, 1003–1012.
May,L.T., Santhanam,U. and Sehgal,P.B. (1991) *J. Biol. Chem.*, **266**, 9950–9955.
Milburn,M.V., Hassell,A.M., Lambert,M.H., Jordan,S.R., Proudfoot,A.E., Graber,P. and Wells,T.N. (1993) *Nature*, **363**, 172–176.
Mott,H.R. and Campbell,I.D. (1995) *Curr. Opin. Struct. Biol.*, **5**, 114–121.
Nicholls,A., Sharp,K.A. and Honig,B. (1991) *Proteins*, **11**, 281–296.
Nishi,R. (1994) *Science*, **265**, 1052–1053.
Owczarek,C.M., Layton,M.J., Metcalf,D., Lock,P., Willson,T.A., Gough,N.M. and Nicola,N.A. (1993) *EMBO J.*, **12**, 3487–3495.
Panayotatos,N., Radziejewska,E., Acheson,A., Pearsall,D., Thadani,A. and Wong,V. (1993) *J. Biol. Chem.*, **268**, 19000–19003.
Panayotatos,N., Everdeen,D., Liten,A., Somogyi,R. and Acheson,A. (1994) *Biochemistry*, **33**, 5813–5818.
Panayotatos,N., Radziejewska,E., Somogyi,R., Hendrickson,W.A., Acheson,A. and McDonald,N.Q. (1995) *J. Biol. Chem.*, **270**, in press.
Pandit,J., Bohm,A., Jancarik,J., Halenbeck,R., Koths,K. and Kim,S.-H. (1992) *Science*, **258**, 1358–1362.
Rajarathnam,K. *et al.* (1994) *Science*, **264**, 90–92.
Robinson,R.C., Grey,L.M., Staunton,D., Vankelecom,H., Vernallis,A.B., Moreau,J.F., Stuart,D.I., Heath,J.K. and Jones,E.Y. (1994) *Cell*, **77**, 1101–1116.

Rozwarski,D.A., Gronenborn,A.M., Clore,G.M., Bazan,J.F., Bohm,A., Wlodawer,A., Hatada,M. and Karplus,P.A. (1994) *Structure*, **2**, 159–173.
Ryden,M., Murray-Rust,J., McDonald,N.Q., Glass,D., Ilag,L.L., Trupp,M., Yancopoulos,G.D., Persson,H. and Ibanez,C.F. (1995) *EMBO J.*, **14**, in press.
Savino,R., Lahm,A., Giorgio,M., Cabibbo,A., Tramontano,A. and Ciliberto,G. (1993) *Proc. Natl Acad. Sci. USA*, **90**, 4067–4071.
Savino,R., Lahm,A., Salvati,A.L., Ciapponi,L., Sporeno,E., Altamura,S., Paonessa,G., Toniatti,C. and Ciliberto,G. (1994) *EMBO J.*, **13**, 1357–1367.
Sendtner,M., Kreutzberg,G. and Thoenen,H. (1990) *Nature*, **345**, 440–441.
Sendtner,M., Stockli,K.A. and Thoenen,H. (1992) *J. Cell Biol.*, **118**, 139–148.
Sendtner,M., Carroll,P., Holtmann,B., Hughes,R.A. and Thoenen,H. (1994) *J. Neurobiol.*, **25**, 1436–1453.
Shapiro,L. *et al.* (1995) *Nature*, **374**, 327–337.
Sprang,S.R. and Bazan,J.F. (1993) *Curr. Opin. Struct. Biol.*, **3**, 815–827.
Stahl,N. and Yancopoulos,G.D. (1993) *Cell*, **74**, 587–590.
Stockli,K.A., Lottspeich,F., Sendtner,M., Masiakowski,P., Carroll,P., Gotz,R., Lindholm,D. and Thoenen,H. (1989) *Nature*, **342**, 920–923.
Ultsch,M., Somers,W., Kossiakoff,A.A. and De Vos,A.M. (1994) *J. Mol. Biol.*, **236**, 286–299.
Ward,L.D, Howlett,G.J., Discolo.G., Yasukawa,K., Hammacher,A., Moritz,R.L. and Simpson,R.J. (1994) *J. Biol. Chem.*, **269**, 23286–23289.
Weis,W., Kahn,R., Fourme,R., Drickamer,K. and Hendrickson,W.A. (1991) *Science*, **254**, 1608–1615.
Williams,L.R., Manthorpe,M., Barbin,G., Nieto-Sampedro,M., Cotman, C.W. and Varon,S. (1984) *Int. J. Dev. Neurol.*, **2**, 177–180.
Zurwaski,S.M., Vega,F.Jr, Doyle,E.L., Huyghe,B., Flaherty,K., McKay, D.B. and Zurawski,G. (1994) *EMBO J.*, **12**, 5113–5119.

Received on February 20, 1995; revised on March 30, 1995